ACS FOOD SCIENCE & TECHNOLOGY

Open Access

pubs.acs.org/acsfoodscitech

Article

Theoretical Insights into Flavonol Solubilization by Deep Eutectic Solvents

Nuria Aguilar, Alfredo Bol-Arreba, Mert Atilhan,* and Santiago Aparicio*

Cite This: ACS Food Sci. Technol. 2023, 3, 1931−1947

Read Online

ACCESS | Metrics & More | Article Recommendations | Supporting Information

ABSTRACT: The low solubility of flavonols in common solvents such as water hinders their extraction from natural sources, solubility, and bioavailability; thus, new solvents are required for the development of flavonols' related technologies and applications. The alternative of deep eutectic solvents for flavonols solubilization is considered in this work through the analysis of the properties and structure of archetypical flavonols (galangin, kaempferol, quercetin, myricetin) in a model deep eutectic solvent (choline chloride:glycerol 1:2) as a function of flavonol concentration through the use of a theoretical approach combining density functional theory and classical molecular dynamics simulations. The solvation and self-aggregation of flavonols in the considered solvent are analyzed through the study of extension and the nature of hydrogen bonding. The complexity of the considered fluids stands on the competing effect for hydrogen bonding development between the components of the solvent, those between the solvent and the flavonols, and the trend to self-aggregation between flavonol molecules, thus determining the solubility of flavonols and the mechanism of solubilization.

KEYWORDS: *deep eutectic solvents, flavonoids, circular economy, density functional theory, molecular dynamics, hydrogen bonding, nanostructuring*

1. INTRODUCTION

Deep eutectic solvents (DESs) have achieved significant relevance in the past few years as they are considered green and sustainable solvents. DESs are formed upon mixing two different compounds, mostly a hydrogen bond donor (HBD) and a hydrogen bond acceptor (HBA), a mixture which at a suitable HBA:HBD molar ratio leads to a melting point (*mp*) depression in comparison with the pure components. The melting point decrease is a result of the hydrogen bond interactions established between the donor and acceptor atoms.[1−4]

The term DES was coined by Abbott and co-workers in 2002[5] when a mixture of choline chloride, ChCl, *mp* = 302 °C and urea, *mp* = 133 °C, in a 1:2 molar ratio was shown to have a melting point at 12 °C. As the formation of hydrogen bonds is the driving force for decreasing the freezing point, a variety of eutectic solvents can be formed by changing the HBA/HBD types as well as the corresponding molar ratio. Their tunable nature is the most important feature of DESs in terms of their technological applications as they can be synthesized as task-specific materials. Therefore, DESs are currently considered for a wide range of technologies including metallurgy and electrodeposition,[6,7] separation and gas capture,[8−13] biocatalysis and organic chemistry applications,[14−18] biomass processing,[19] pharma,[20−26] and natural product extractions.[27,28] The majority of the basic and applied DESs research is focused on Type III DESs, with particular attention given to DESs based on ChCl as HBA and nitrogen-based reactants, alcohols, or carboxylic acids as HBDs. DESs containing polyols exhibit the lowest melting point.[29] Among them, glyceline (ChCl 1:2 glycerol) is a common DES used in very different applications.[1] ChCl is a nontoxic, biodegradable, biocompatible, and cheap salt used as a nutritional additive,[30] and glycerol is a byproduct of chemical reactions of oils and fats in the soap and biodiesel industries used in food and pharmaceutical manufacturing. As glycerol cannot be used as fuel, its excess is usually treated as a waste product.[31,32] Thus, glyceline can be considered as a circular economy valorization opportunity for residual glycerol being a nonflammable, nontoxic, and biodegradable DES with a melting point of −40 °C (*mp* of glycerol: 18 °C)[33,34] and relatively low viscosity when compared to other DES based on Gly as HBD (281 cP at 298 K). Because of the low viscosity, glyceline shows a high electrical conductivity (985 μS cm^{-1} at 298 K).[35]

ChCl-based DES, and specially glyceline, are extensively used in high-purity extraction and separation of bioactive compounds from natural products[36] such as phenolic compounds (PC).[37] Natural PCs are present in the majority of plants as a secondary metabolite, protecting the plant against drastic climate conditions and pathogens. They are widely studied as they have interesting biological activities as antioxidant, anti-inflammatory, antimicrobial, anticancer, and analgesic.[38] Among natural PC, flavonoids are used in the pharmaceutical, cosmetic, and food industries because of their antioxidant and potential anticancer activity and are commonly

Received: July 20, 2023
Revised: September 13, 2023
Accepted: September 14, 2023
Published: October 18, 2023

extracted using organic or petroleum-based solvents as their planar structure (π-stacking) prevents them from dissolving in water. In order to avoid the environmental and human damage caused by these types of solvents for PCs extraction, DESs are proposed as an alternative extractant as they have been proven to be suitable for flavonoids extractions.[39,40] The basic flavonoid structure contains two aromatic C6 rings (namely, A and B) linked through a heterocyclic pyran or pyrone ring (C). Flavonols (FLAVs) are a type of flavonoids in which the ring B (catechol) is attached to position 2 of ring C, the latter linked to a hydroxyl group in position 3, Figure 1. FLAVs can

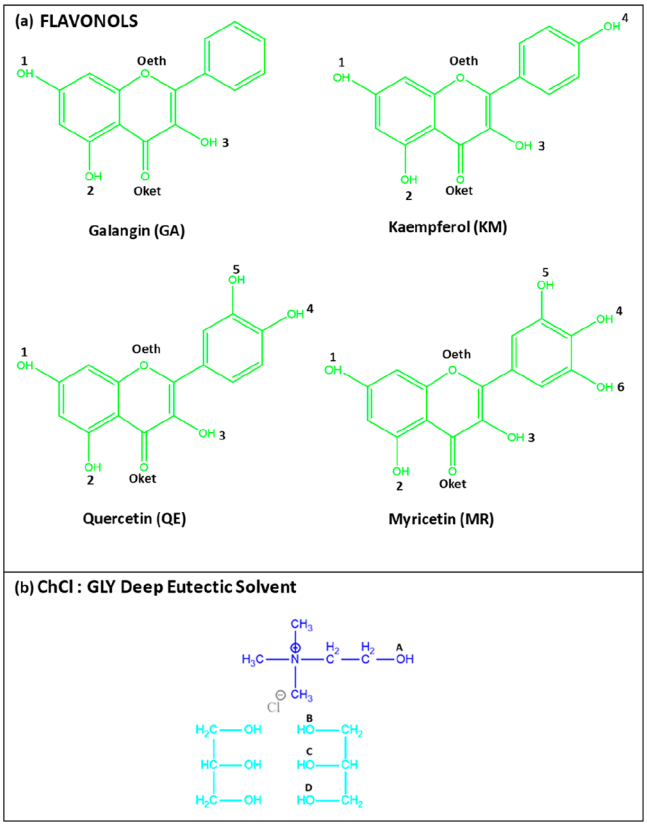

Figure 1. (a) Flavonols and (b) DES considered in this work. Atomic labeling used along this work is indicated.

be subsequently classified by considering the number and position of hydroxyl substituents on ring B, affecting their properties and characteristics. Fruits and vegetables are the main sources of FLAVs for humans as they cannot be synthesized.[41−44]

The extraction of different FLAVs by ChCl-based DESs has been extensively evaluated by experimental methods[45−52] in order to optimize the extractions conditions (i.e., liquid/solid ratio, temperature, pressure and time extraction, water content) from a variety of techniques and FLAV vegetal sources. DESs have been proven to be an ideal green extractant for these types of molecules, standing out from the classical organic solvents.[53] Moreover, FLAVs are efficiently recovered from the DES, which can then be reutilized. Despite the vast quantity of experimental information, there is a lack of understanding of the mechanism of interaction and solubilization of the FLAVs in DESs, possibly because of the large number of variables affecting the yield of extraction, the multiple techniques, and the huge amount of available potential solvents. Multiscale molecular modeling is a powerful tool to systematically study the structure, properties, and mechanisms of interaction of a large number of compounds, mixtures, and operation conditions from nano- to macroscale. Likewise, computational chemistry methods have been proven to be useful in fathoming the pivotal role of HBA/HBD hydrogen bonds in the structures and physicochemical properties of DESs.[54,55] Thus, the changes occurring in the hydrogen bond network in both solvent and solutes must be evaluated when DESs molecules interact with FLAVs, as the latter present several donor/acceptor sites (i.e., ether, ketone, and hydroxyl groups) in order to comprehend the driving force for the solubilization process. Moreover, simulating the dynamics of the fluid phase of the mixture at different conditions, i.e., temperature, pressure, HBA:HBD molar ratio, and molar fraction of FLAVs, allows one to identify the best extraction conditions.

In the present work, two computational approaches have been applied to study the interactions at the molecular level between four types of FLAVs and glyceline DES: quantum chemistry (DFT) and classical molecular dynamics (MD). The selected FLAVs (galangin, GA; kaempferol, KM; quercetin, QE, myricetin, MR) have been previously considered in experimental studies.[56−59] Furthermore, Li et al. reported the structures, interaction, and hydrogen bond lengths between KM and QE and DESs based on caffeic acid, ethylene glycol, and choline chloride obtained with DFT.[60] The aim of the present work is to deepen the knowledge of these intermolecular interactions, which are at the roots of the solubility of different flavanols in glyceline from both quantum and classical molecular simulations.

2. METHODS

2.1. Density Functional Theory Calculations. The initial structures for the involved molecules (ChCl, GLY, and FLAVs) composing the DES (glyceline) + FLAV mixtures were built with the Avogadro program.[61] To study all of the possible intermolecular interactions (hydrogen bonding) in the considered mixtures, 72 different clusters were built, considering all of the possible interaction sites for hydrogen bond interactions between the FLAV and DES components. According to the atomic labeling in Figure 1, the DES−FLAV clusters were named in a systematic way as follows: *FLAV _ O atom in FLAV _ O atom in DES*, e.g., GA_1A, stands for DES−GA 1:1 cluster considering the interaction between the OH(1) site in GA and the A site in DES (OH group in Ch), Figure 1. All the monomers and the 72 DES−FLAV clusters were subjected to geometrical optimization using DFT with ORCA software[62] using the hybrid Generalized Gradient Approximation (hybrid-GGA) and the wB97X functional[63] with balanced polarized triple-ζ basis set (def2-TZVP)[64] and def2-J auxiliary basis set.[65] The binding energy between the FLAV and the DES, ΔE, for each DES−FLAV cluster was calculated as follows:

$$\Delta E = E_{(\mathrm{DES-FLA})} - E_{\mathrm{DES}} - E_{\mathrm{FLA}} \quad (1)$$

with the energy for the DES calculated as

$$E_{\mathrm{DES}} = E_{\mathrm{DES}} - E_{\mathrm{ChCl}} - 2E_{\mathrm{Gly}} \quad (2)$$

where $E_{(\mathrm{DES-FLA})}$ stands for the energy of the system DES−FLA 1:1, E_{DES} for the energy of the DES (calculated as the difference between the energy of the system ChCl:GLY 1:2 and the energy of the isolated molecules, ChCl and Gly), and E_{FLA} for the energy of the isolated FLA. Topological analysis of the intermolecular interactions for the optimized structures of DES-FLA systems was carried out according to the quantum theory of atoms-in-molecules (QTAIMs) (Bader's AIM theory)[66] with Multiwfn software.[67] This analysis was applied for the considered interaction regions (hydrogen bond donor and

https://doi.org/10.1021/acsfoodscitech.3c00281
ACS Food Sci. Technol. 2023, 3, 1931−1947

acceptor sites) by using bond critical points (BCPs). These are characterized with their corresponding values of electron density (ρ) and the Laplacian of electron density, $\nabla^2\rho$. Likewise, the Core−valence bifurcation index (CVB[68]) was calculated from the electron localization function, ELFs, for the corresponding hydrogen bonding sites. Further analysis of intermolecular interactions was carried out considering non-covalent interaction (NCI) analysis to display the strength and nature of weak interactions.[69]

2.2. Classical Molecular Dynamics Simulations. Classical molecular dynamics (MD) simulations for the selected DES + FLAV liquid systems were carried out with the MDynaMix 5.2.8. program.[70] The initial cubic simulation boxes were built with the PACKMOL program containing a total of 500 DES units (500 Ch, 500 Cl, and 1000 glycerol molecules, resembling the composition of ChCl: Gly (1:2) DES) and a variable number of FLAV molecules depending on the FLAV molar fraction considered for each system (x = 0.1, 0.2 and 0.3, where x stands for FLAV mole fraction), Table 1. The force field parametrizations used in the present work are reported in Table S1 (Supporting Information). The parameters reported were obtained by applying the Merck molecular force field via the SwissParam database,[71] excluding the atomic charges that were gathered from ChelpG charges[72] calculated within the DFT simulations of isolated monomers as obtained in this work.

Two-step production was performed for MD simulations for all the considered systems: (i) the initial simulation boxes aforementioned, i.e., the boxes built with PACKMOL, were submitted to MDynaMix software for a 5 ns long simulation in the NVT ensemble at 303 K for equilibration purposes followed by (ii) 30 ns long simulations in the NPT ensemble at 303 K and 1 bar for production runs, assured by the constancy of the total potential energy and density. For all the MD simulations, temperature and pressure were controlled with the Nose−Hoover method.[73] The Ewald method[74] (10 Å of cutoff radius) was applied for treating Coulombic interactions, while Lennard−Jones interactions were handled with 10 Å cutoff distance. The Tuckerman−Berne double time step algorithm[75] was used for solving the equations of motion (1 and 0.1 fs for long- and short-time steps) and Lorentz−Berthelot mixing rules for cross terms. The visualization, analysis, and postprocessing of MD trajectories were carried out using VMD[76] and TRAVIS.[77]

Table 1. Systems Considered for MD Simulations of x FLAV + $(1 - x)$ DES Mixtures as a Function of FLAV Content at 303 K and 1 bar[a]

	N			
x	Ch	Cl	GLY	FLAV
0.1	500	500	1000	56
0.2	500	500	1000	125
0.3	500	500	1000	214

[a]N stands for the number of molecules of each type for each mixture composition.

3. RESULTS AND DISCUSSION

3.1. DFT Results. *3.1.1. Energy Results: Interactions Strength.* The main factor governing the FLA solubilization into the considered DES, and thus the DES performance for FLA extraction from natural sources, stands on the ability of FLA to develop effective hydrogen bonding with the DES

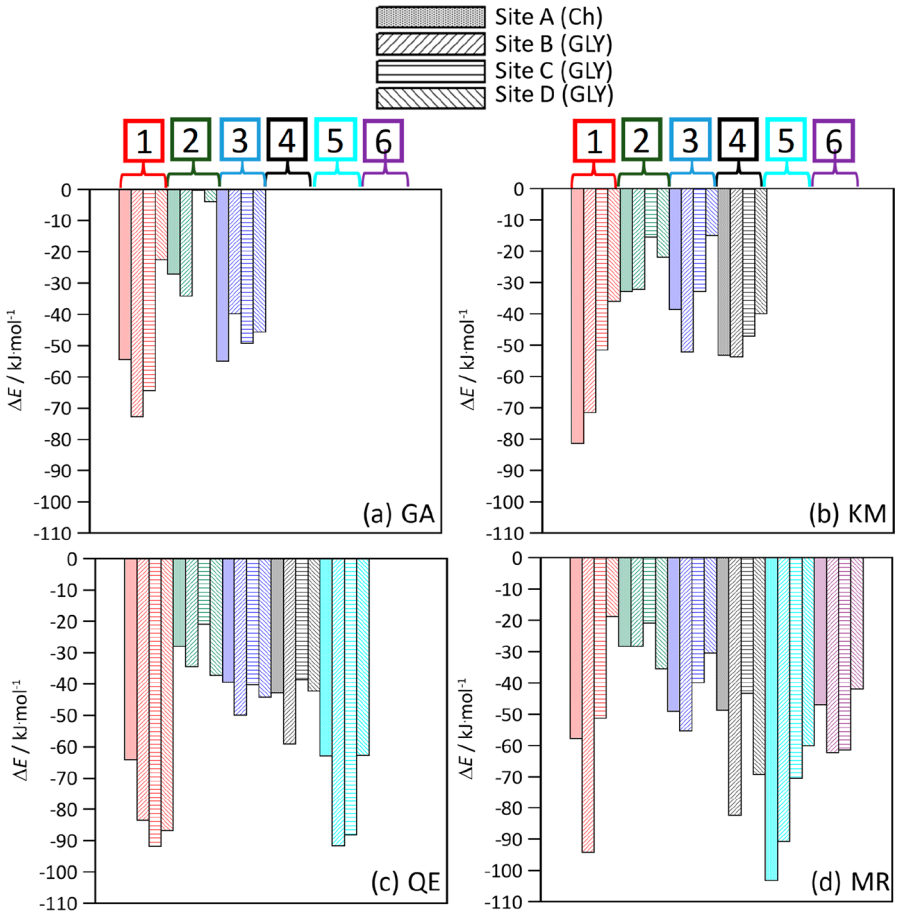

Figure 2. (a−d) Interaction energy, ΔE, from DFT optimization of DES−FLAV clusters for different interacting positions with atomic labeling as in Figure 1.

https://doi.org/10.1021/acsfoodscitech.3c00281
ACS Food Sci. Technol. 2023, 3, 1931−1947

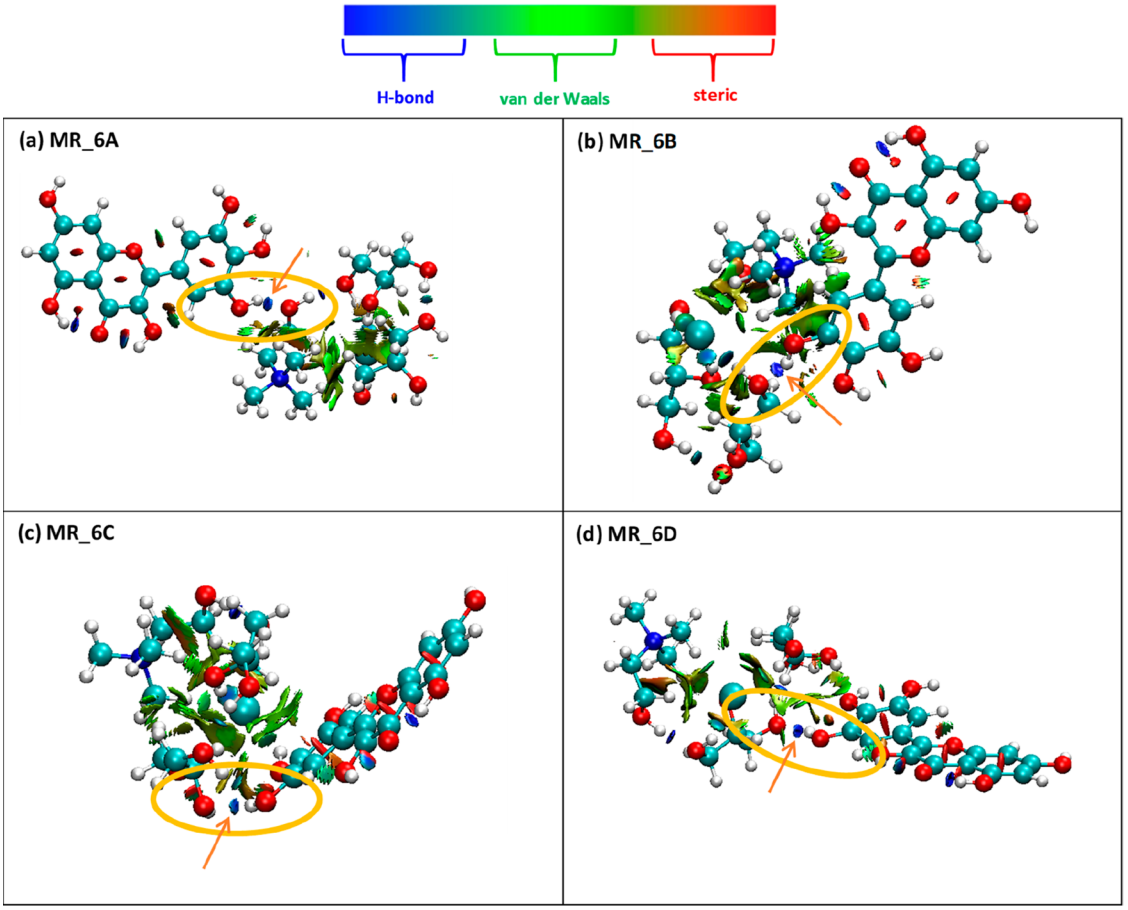

Figure 3. (a–d) NCI analysis of MR–DES interacting pairs for different acceptor sites in DES. Atomic labeling as in Figure 1.

components (HBA and HBD, Ch, and GLY). The ChCl:GLY DES has four hydrogen bonding molecular sites: (i) the hydroxyl group in Ch cation, labeled A in Figure 1b and (ii) the three hydroxyl groups in the GLY molecule, labeled B, C and D in Figure 1. These hydroxyl sites in the DES structure may act as both hydrogen bond donors and/or acceptors. The hydroxyl groups in GLY take part, at least partially, of the hydrogen bonding with the Cl anion in ChCl. The considered FLAVs have between three (GA) and six (MR) hydroxyl groups placed at different positions of the aromatic rings as well as a single ketone oxygen and ether oxygen. The FLAVs' hydroxyl groups may also act as both hydrogen bond donors as well as acceptors. In contrast, the oxygen atoms in the ketone and ether groups may only act as acceptors. Therefore, the presence of the FLAVs in the DES liquid structure should lead to changes in the hydrogen bonding in extension, nature, and strength. The reason is that upon FLAVs solubilization, competing hydrogen bonding will be present. Four types can be distinguished: (i) DES internal (HBA–HBD), (ii) DES–DES, (iii) DES–FLAV, and (iv) FLAV–FLAV. Therefore, to analyze the nature of the DES–FLAV hetero association via hydrogen bonding, DFT calculations of minimal DES–FLAV 1:2 clusters were carried out. The available interaction sites were considered to quantify the strength and nature of these interactions that eventually led to the solubilization of FLAV.

Results in Figure 2 report the ΔE for the four considered FLAVs as well as for all of the possible interaction sites (pairs). The first conclusion inferred from the results in Figure 2 is that although ΔE values for all the possible DES–FLAV pairs are negative, i.e., hydrogen bonding is possible for all the available sites and interacting pairs, the strength of these interactions is remarkably different. The values of ΔE are in the range of −5 to −103 kJ mol^{-1}; thus, preferential interaction sites and types of hydrogen bonds should be present in the DES–FLAV mixed fluids. The general ordering of ΔE according to the hydroxyl site in the FLAVs is site 1 ∼ site 5 > site 6 ∼ site 4 > site 3 > site 2. Therefore, interactions through hydroxyl groups in the cathecol moiety (sites 4, 5, 6) are stronger than those through groups in the benzopyran sites, especially for sites 3 and 2, with the exception of site 1. The weakest hydrogen bond interaction is reported for site 2 as a consequence of the keto–enol intramolecular hydrogen bond formed between the hydroxyl donor and the ketone acceptor, depicted in Figure 3a as a blue spot between those groups. Regarding the effect of the available sites in the considered DES (A–D sites), the effect is not systematic and seems to be less important than the type of FLAV hydroxyl group.

3.1.2. Bond Topology: Electronic Properties Results. The nature of DES–FLAV hydrogen bonds is analyzed through QTAIM theory and reported in Table 2 for the ρ and $\nabla^2\rho$ in the BCPs appearing along the bond path corresponding to each hydrogen bond. In all cases, a BCP is inferred between the corresponding hydrogen bond donor and acceptor atoms, confirming the interaction's development. The nature and strength of a developed hydrogen bond as those for DES–FLAV may be analyzed considering the values of ρ and $\nabla^2\rho$. Koch et al.[78] showed that ρ and $\nabla^2\rho$ for BCPs corresponding to hydrogen bonding paths are in the 0.002 to 0.034 au and

https://doi.org/10.1021/acsfoodscitech.3c00281
ACS Food Sci. Technol. 2023, 3, 1931–1947

Table 2. QTAIM Analysis of BCPs along the Hydrogen Bonding Site Corresponding to FLAV−DES Interactions for Different Donor and Acceptor Sites[a]

position	ρ/a.u.	$\Delta^2\rho$/a.u.	CVB	ΔE/kJ·mol^{-1}	position	ρ/a.u.	$\Delta^2\rho$/a.u.	CVB	ΔE/kJ·mol^{-1}
GA_1A	0.040	0.125	−0.028	−54.5	**QE_1A**	0.032	0.105	−0.007	−64.1
GA_1B	0.049	0.124	−0.070	−72.9	**QE_1B**	0.025	0.083	0.011	−83.7
GA_1C	0.036	0.109	−0.021	−44.9	**QE_1C**	0.030	0.101	0.003	−92.0
GA_1D	0.037	0.120	−0.017	−64.4	**QE_1D**	0.031	0.101	−0.001	−86.9
GA_2A	0.015	0.068	0.061	−27.3	**QE_2A**	0.015	0.066	0.063	−28.0
GA_2B	0.016	0.072	0.061	−34.2	**QE_2B**	0.036	0.115	−0.012	−34.5
GA_2C	0.005	0.020	0.086	−0.4	**QE_3A**	0.026	0.100	0.026	−39.5
GA_2D	0.019	0.081	0.053	−4.0	**QE_3B**	0.040	0.118	−0.032	−49.9
GA_3A	0.033	0.116	0.000	−55.1	**QE_3C**	0.038	0.116	−0.023	−40.3
GA_3B	0.038	0.117	0.002	−39.9	**QE_3D**	0.039	0.116	−0.027	−44.2
GA_3C	0.039	0.118	−0.027	−49.3	**QE_4A**	0.033	0.114	−0.003	−42.9
GA_3D	0.038	0.117	−0.023	−45.8	**QE_4B**	0.040	0.118	−0.033	−59.1
KM_1A	0.037	0.120	−0.017	−81.5	**QE_4C**	0.029	0.102	0.009	−38.7
KM_1B	0.041	0.118	−0.038	−71.7	**QE_4D**	0.036	0.111	−0.019	−42.2
KM_1C	0.022	0.079	0.025	−51.7	**QE_5A**	0.028	0.098	0.009	−62.9
KM_1D	0.041	0.116	−0.038	−36.1	**QE_5B**	0.039	0.116	−0.028	−91.7
KM_2B	0.015	0.070	0.064	−32.3	**QE_5C**	0.030	0.101	0.003	−88.2
KM_2C	0.013	0.060	0.067	−15.7	**QE_5D**	0.032	0.106	−0.004	−62.9
KM_2D	0.013	0.052	0.064	−22.1	**MR_1A**	0.036	0.117	−0.013	−57.9
KM_3A	0.024	0.096	0.031	−38.7	**MR_1B**	0.035	0.107	−0.015	−94.2
KM_3B	0.036	0.126	−0.005	−52.2	**MR_1C**	0.040	0.125	−0.024	−51.4
KM_3C	0.038	0.112	−0.027	−33.1	**MR_1D**	0.036	0.114	−0.016	−18.9
KM_3D	0.037	0.114	−0.021	−15.1	**MR_2A**	0.015	0.068	0.061	−28.4
KM_4A	0.038	0.122	−0.021	−53.3	**MR_2B**	0.020	0.090	0.049	−28.4
KM_4B	0.037	0.113	−0.022	−53.8	**MR_2C**	0.014	0.063	0.067	−21.1
KM_4C	0.034	0.106	−0.014	−47.3	**MR_3A**	0.036	0.121	−0.006	−49.2
KM_4D	0.032	0.108	−0.002	−40.0	**MR_3B**	0.043	0.130	−0.032	−55.4
					MR_3C	0.039	0.120	−0.024	−39.9
					MR_3D	0.035	0.105	−0.008	−30.5
					MR_4A	0.034	0.104	−0.013	−48.9
					MR_4B	0.040	0.124	−0.028	−82.4
					MR_4C	0.040	0.112	−0.039	−43.5
					MR_4D	0.038	0.116	−0.021	−69.3
					MR_5A	0.031	0.105	0.002	−103.3
					MR_5B	0.037	0.113	−0.023	−90.7
					MR_5C	0.032	0.108	−0.004	−70.4
					MR_5D	0.041	0.126	−0.031	−60.2
					MR_6A	0.033	0.115	0.001	−47.0
					MR_6B	0.040	0.118	−0.031	−62.3
					MR_6C	0.029	0.101	0.006	−61.4

[a]Atomic labelling as in Figure 1. ρ stands for electron density and $\nabla^2\rho$ stands for Laplacian of the corresponding density, for the BCP between the FLAV and DES at each interacting site. The CVB index is also reported for the same interaction sites.

0.024 to 0.139 au, for ρ and $\nabla^2\rho$ respectively, with larger values corresponding to stronger interactions. The analysis of hydrogen bonds according to ρ and $\nabla^2\rho$ shows a large diversity of values, which correspond to the differences in the strength of the interactions, as reported in Figure 2. For example, interacting pairs like GA_2C or GA_2D having very low ΔE lead to ρ and $\nabla^2\rho$ close to the lower limit of the ranges reported by Koch et al.;[78] i.e., weak hydrogen bonds are topologically characterized by low charge density at the corresponding interacting site characterized through the corresponding BCPs. Nevertheless, as most of the possible hydrogen bonds correspond to large ΔE (Figure 2), the QTAIM analysis led to ρ and $\nabla^2\rho$ close to or even slightly above the top range limits, which indicate very effective interactions considering the applied topological criteria. The second criterion used to analyze the developed hydrogen bonds is on the CVB index inferred from ELF analysis, Table 2. The use of CVB for the quantification of hydrogen bonds is based on the consideration that the lower (i.e., going negative) this index, the stronger the interaction. The CVB values reported in Table 2 are mostly negative, corresponding to very strong hydrogen bonds, whereas those that are positive correspond to weaker interactions. Therefore, the CVB analysis indicates a strong hydrogen bond for most of the possible interaction pairs.

3.1.3. Geometrical Results. The analysis of DES−FLAV interactions is also carried out through the NCI method, with results for MR−DES interactions reported in Figure 3 (analogous results inferred for the remaining FLAVs and interacting sites). Figure 3 shows NCI analysis of the DES−MR interaction for different sites in the DES structure. First of all, the formation of DES−MR interaction does not affect the

https://doi.org/10.1021/acsfoodscitech.3c00281
ACS Food Sci. Technol. 2023, 3, 1931−1947

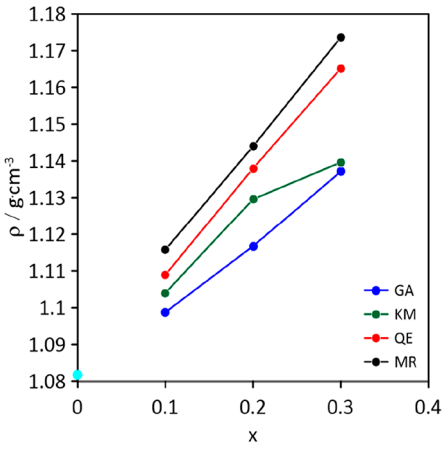

Figure 4. MD predicted density for x FLAV + $(1 - x)$ DES mixtures as a function of FLAV content at 303 K and 1 bar. Cyan circle shows the density for pure DES.

internal structure of the DES, as inferred from the large spots inferred for all the possible interacting sites; i.e., DES−FLA interaction is developed in available sites without disrupting the HBA (ChCl)−HBD (GLY) hydrogen bonding. For all the considered hydrogen bonding sites in the DES (sites A to D), the NCI analysis shows the development of blue spots largely localized along the direction joining hydrogen bonding donor and acceptor sites, which corresponds to strong hydrogen bonds in agreement with QTAIM, ELF, and interaction energy results. Likewise, the results show the development of NCI green areas corresponding to van der Waals interactions in the regions between MR (FLAV) and the DES, especially for the B position in the DES, which should contribute to strengthening the DES−FLAV interaction beyond the specific and localized hydrogen bonds, leading to the very large ΔE values reported in Figure 2d.

Therefore, the combined analysis of the possible hydrogen bonds through the strength of interaction, topology (QTAIM), electronic properties, (CVB, ELF), and geometry (NCI) indicates how the considered FLAVs are extremely versatile hydrogen bonding molecules; they can interact efficiently with all the available hydrogen bonding sites in the considered DES. Moreover, the development of DES−FLAV hydrogen bonding does not remarkably disrupt the properties, of the HBA−HBD interactions leading to the main DES properties, which is also a remarkable feature for considering FLAVs solubility.

3.2. MD Results. *3.2.1. Density and Hydrogen Groups in the FLAVs.* The previous study has probed and analyzed the developed DES−FLAV intermolecular interactions using a minimal clusters model. Nevertheless, the corresponding DES−FLAV liquid phases should have effects and interactions beyond the short-range ones considered in this model, and consequently, MD simulations were carried out. The values of MD predicted density reported in Figure 4 show a large effect because of the presence of FLAVs in DES depending on the type of FLAV and on their concentrations. The density values reported in Figure 4 show an increase of the density as the number of hydroxyl functional groups in the FLAV, e.g., myricetin (MR) has six hydroxyl functional groups, whereas quercetin (QE) has five (Figure 1), then the density reported for MR systems is higher than that reported for QE systems. The reason for yielding a higher density is related to the extension of the hydrogen bond network, stronger as the number of possible sites increases, as DFT results have probed. Likewise, as the FLAV concentration rises, the densification upon FLAV solubilization increases as the number of hydrogen bond donor and acceptor atoms multiply in the fluid. Therefore, the densification effect is directly correlated with the number of available hydroxyl groups in the FLAV, i.e., larger solubility as the number of hydroxyl groups increases in the FLAV molecule and/or inside the fluid simulated (molar fraction of the same FLAV).

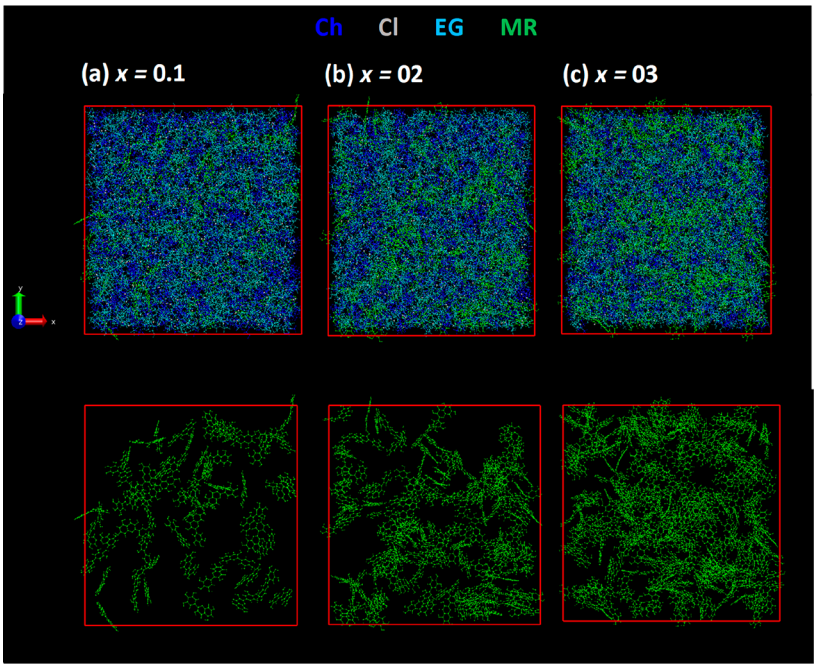

Figure 5. Snapshots for x MR + $(1 - x)$ DES mixtures as a function of the FLAV content at 303 K and 1 bar. The top row shows all of the molecules present in the mixture, and the bottom row shows only MR.

https://doi.org/10.1021/acsfoodscitech.3c00281
ACS Food Sci. Technol. 2023, 3, 1931−1947

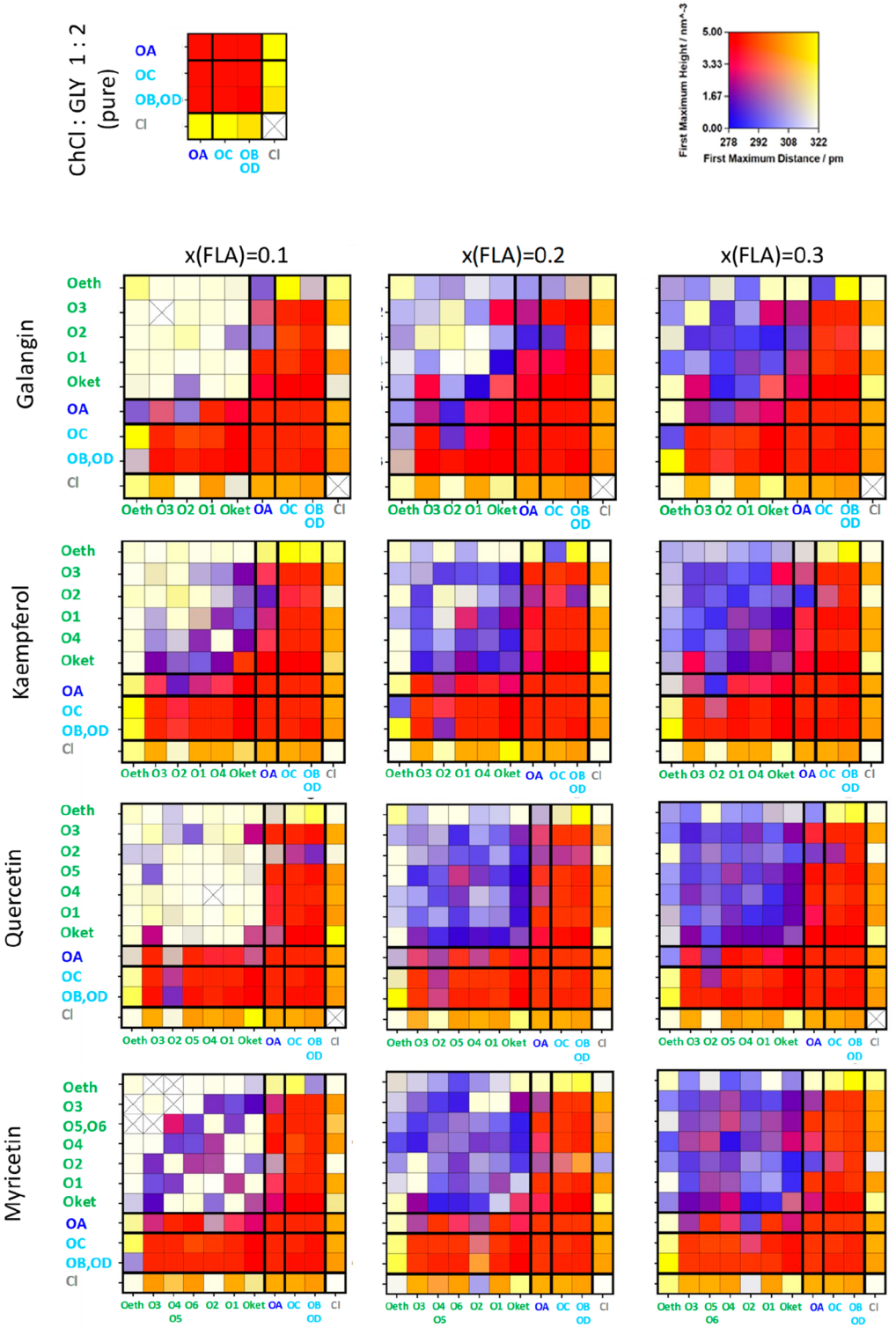

Figure 6. Connection matrix analysis for possible hydrogen bonds for x FLAV + $(1 - x)$ DES mixtures as a function of the FLAV content at 303 K and 1 bar. Rows and columns represent all possible donor−acceptor sites for hydrogen bonding. Atom labeling as in Figure 1. The color of each square corresponds to the intensity and distance of the first maximum in the corresponding radial distribution functions with the color scale indicated in the panel on the top right corner.

3.2.2. Liquid Internal Structure: Solubilization of FLAVs in DES. The distribution of FLAV molecules in the DES solvent upon solubilization is first analyzed through the snapshots reported for DES−MR in Figure 5. These results show a homogeneous distribution of MR(FLAV) molecules in the DES liquid (Figure 5a). That is to say, a fluid distribution is dominated by the DES liquid structure with minor structural disruption because of the presence of MR(FLAV) molecules. But as the FLAV content increases, an MR(FLAV)-dominated fluid structuring emerges with the formation of local heterogeneities that can be inferred as MR(FLAV) self-clustering predicting the limit of solubility into the considered

https://doi.org/10.1021/acsfoodscitech.3c00281
ACS Food Sci. Technol. 2023, 3, 1931−1947

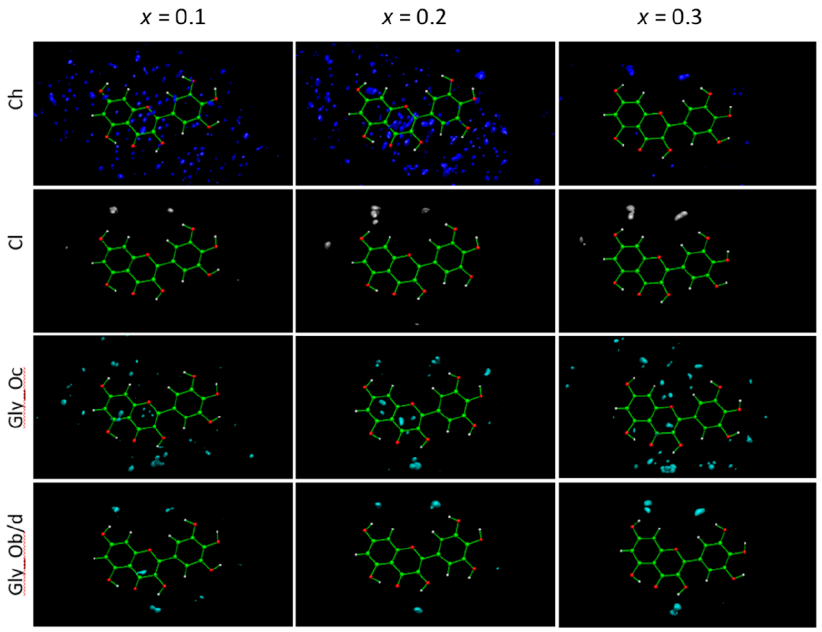

Figure 7. Spatial distribution functions, SDFs, of DES components around a central MR molecule for x MR + $(1 - x)$ DES mixtures as a function of the FLAV content at 303 K and 1 bar. Atom labeling as in Figure 1.

DES. The analysis of the intermolecular interactions in the DES−FLAV mixed systems was also carried out using site−site radial distribution functions (RDFs). Considering the large number of possible donor−acceptor sites (Figures 1 and 2), these RDFs were systematically analyzed and arranged considering the so-called connection matrix (*cmat*), a function available at TRAVIS software.[77] The *cmat* depicts the combination of the first maximum height and the first maximum distance for the interacting pairs chosen, the same information as for a classical RDF where the first peak is characterized by its distance and height, but the *cmat* function systematizes the results as a contact matrix in which a color code indicates the hydrogen bond strength in terms of height and distance of the first maximum (first peak of the RDF) for all pairs simultaneously. The color code provided by TRAVIS software is shown at the top of Figure 6 allowing the visualization and comparison of the nature and intensity for all the relevant interactions in the DES−FLAV systems, Figure 6. For the first maximum height (height of the first RDF peak), the color varies from red to yellow as the first maximum distance grows from its minimum, 278 pm, to its maximum value, 322 pm. Complementary, the color changes from blue to red for the closest peak of the RDFs (the minimum value of the first maximum distance, 278 pm for the *cmat* reported) as the first maximum height increases from 0.0 nm^{-3} to its highest value, 5.0 nm^{-3}. Therefore, the color code indicates the strength of the hydrogen bonds under study; e.g., the color for the strongest hydrogen bond interaction, considering the oxygen atom as a donor and acceptor, is red as the distance and height correspond to the minimum and the maximum respectively. The first row of *cmat* results in Figure 6 shows the behavior of neat (in the absence of FLAVs) DES, which shows the HBA (A sites in Ch and Cl anion) interactions with HBD (B, C, and D sites in GLY molecules), as probed by the red and yellow spots. Therefore, the neat DES is characterized by short GLY−Ch interactions and slightly larger GLY−Cl interactions, which would correspond to the development of hydrogen bonds inside the DES minimal cluster (Cl−GLY interactions) as well as between neighboring DES clusters (GLY−GLY). Likewise, GLY−GLY hydrogen bonding is also inferred, as indicated by the strong red spots. The lower right corner region in the *cmat* diagrams corresponds to DES−DES self-interaction, and its comparison with values on the top row of Figure 6 allows us to infer the changes in DES−DES hydrogen bonding when FLAVs are solubilized. The first effect that can be inferred from results in Figure 6 is the change in hydrogen bonds corresponding to DES self-interaction. The reported *cmat* results indicate minor changes in DES self-hydrogen bonding; the results indicate that the interactions between the Cl anion and GLY are characterized by shorter distances than in neat DES (*cmat* color code evolving from yellow in neat DES to orange in DES−FLAV systems), whereas the opposite effect is inferred for Ch−Ch, GLY−Ch, and GLY−GLY interactions, which are slightly increased in terms of distances (*cmat* color code evolving from red in neat DES to orange in DES−FLAV systems). This minor change is produced for all of the considered FLAVs and appears even for the lowest FLAV content, with minor changes even for the largest FLAV concentration, with the *cmat* indicating that hydrogen bonds between DES components are maintained in the presence of the FLAVs. For the DES−FLAV interactions (*cmats* in the lower left corner), results indicate that FLAV molecules are preferentially interacting with hydroxyl groups of GLY molecules (red spots), which agrees with the strong hydrogen bonding as inferred from DFT results (Figure 2). Therefore, FLAVs interactions with DES are preferential to the hydroxyl−hydroxyl type. Regarding the FLAV−FLAV interactions (*cmats* in the upper left corner), the results indicate a large concentration effect, with the blue spots indicating the formation of interactions increasing as the FLAV content increases for all the considered FLAVs. Therefore FLAVs are more self-associated as the number of FLAV molecules increases. This effect agrees with the trend to form FLAV clusters for a large FLAV content, as reported in Figure 5. Regarding the type of hydrogen bonding for FLAV clustering, *cmat* results indicate the prevailing interaction through

https://doi.org/10.1021/acsfoodscitech.3c00281
ACS Food Sci. Technol. 2023, 3, 1931−1947

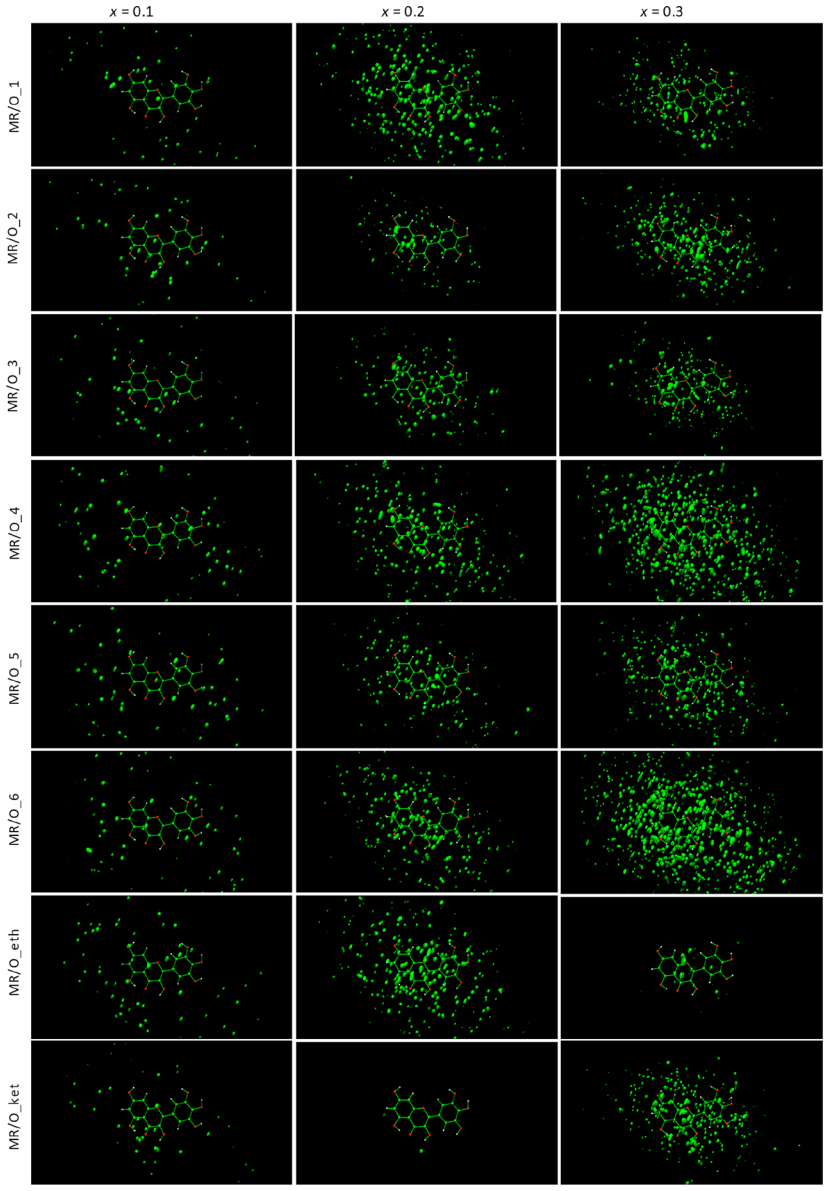

Figure 8. Spatial distribution functions, SDFs, of O atoms in MR around a central MR molecule for x MR + $(1 - x)$ DES mixtures as a function of FLAV content at 303 K and 1 bar. Atom labeling as in Figure 1.

hydroxyl groups, although hydrogen bonds are also formed through ketone and ether sites.

3.2.3. Liquid Internal Structure: Solvation. The particular spatial distribution around FLAV molecules, i.e., solvation structuring, is analyzed in Figures 7 and 8 by considering the spatial distribution functions (SDFs) around a central MR molecule (analogous results are inferred for the remaining FLAVs considered in this work). The Ch cations (Figure 7) show a scattered distribution around the central MR molecule, although decreasing as MR content increases, leading to concentrated spots around hydroxyl groups in positions 1 and 4 of the MR. In the case of the Cl anion (Figure 7), they are also localized around the 1 and 4 hydroxyl groups of the FLAV, which is correlated with the trend of the Ch cation as Ch−Cl interacts through strong Coulombic interactions. The distribution of GLY hydroxyl groups (Figure 7) is almost the same for both terminal and central groups in GLY, being localized around most of the MR (FLA) hydroxyl groups, in agreement with the reported *cmat* and DFT results. Therefore, all the available hydroxyl groups in the MR(FLAV) interact with the available hydrogen bonding sites in the DES components.

Regarding the distribution of MR(FLAV) around central MR(FLAV), Figure 8, the reported results indicate scattered distribution around all of the available hydroxyl groups, i.e., no preferential interaction sites. These results indicate FLAV−FLAV self-aggregation, which increases for all of the possible hydrogen bonding sites as the FLAV content increases, which confirms the trend of FLAV molecules to self-clustering on the top of the solubility range.

3.2.4. Hydrogen Bonding Analysis. The formation of hydrogen bonding was confirmed through DFT and MD structural analysis. The extension of hydrogen bonding is reported in Figures 9 and 10. The total number of hydrogen bonds per molecule present in the DES−FLAV solutions is reported in Figure 8 for all of the considered FLAVS and compositions. All the considered FLAVs show the same trends in the total number of hydrogen bonds: the type of FLAV has a

https://doi.org/10.1021/acsfoodscitech.3c00281
ACS Food Sci. Technol. 2023, 3, 1931−1947

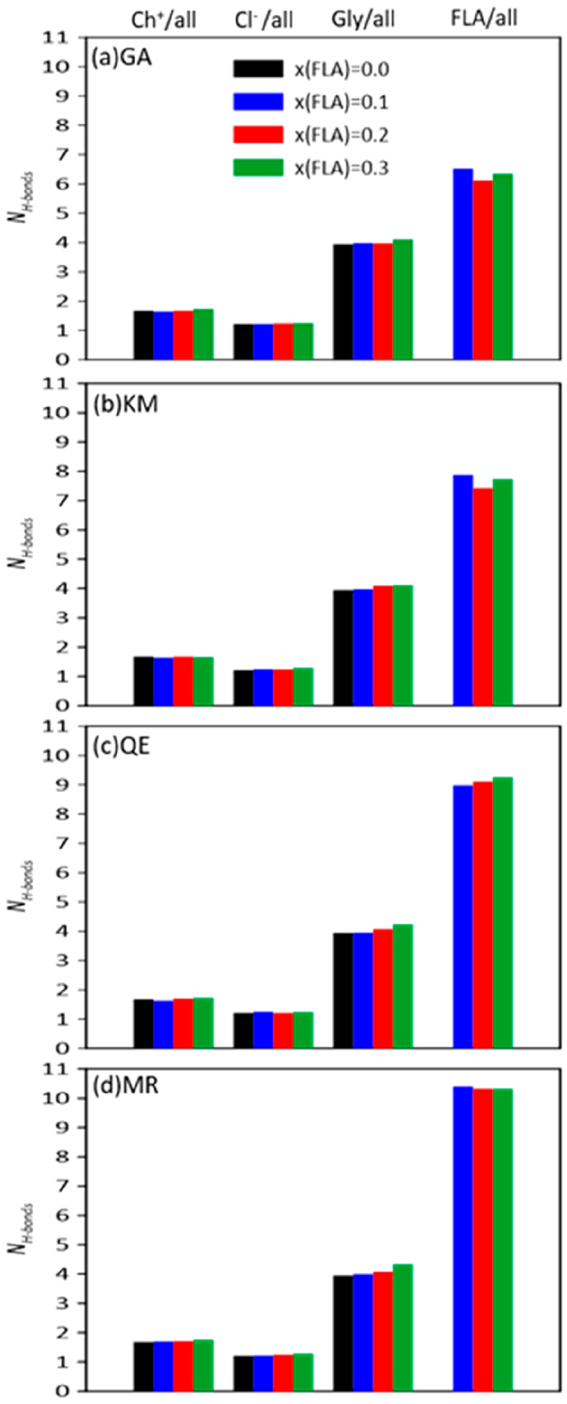

Figure 9. (a−d) Total number of hydrogen bonds, $N_{\text{H-bonds}}$ (considering all the possible donor−acceptor sites for each molecule), for x FLAV + $(1 - x)$ DES mixtures as a function of FLAV content at 303 K and 1 bar.

minor effect on the hydrogen bond structuring, Figure 9. Not surprisingly, the number of hydrogen bonds per molecule follows the ordering: Cl < Ch < GLY < FLA. This effect corresponds to the difference in the number of hydrogen bonding sites which is larger for the considered FLAVs. Likewise, the total number of hydrogen bonds established molecule increases as GA < KM < QE < MR, which agrees with the number of available hydroxyl sites in the FLAV and confirms that all of these hydroxyl sites are able to develop hydrogen bonds. Moreover, the FLAV content has a negligible effect on the number of hydrogen bonds per molecule. The evolution of the different types of hydrogen bonds is analyzed in Figure 10 in which all of the possible pairs are considered. For most of the considered pairs, the composition effect is almost negligible with the exception of Ch−FLAV, Cl−FLAV, and GLY−FLAV, which increase with the FLAV content, indicating that DES−FLAV hetero association is more extensive as the FLAV content is larger. Another remarkable feature is the extension of DES self-association. The number of hydrogen bonds involving DES components shows a small decrease with increasing FLAV content, with the largest decrease for Cl−GLY and GLY−GLY interactions, which is produced by the increase of DES−FLAV interactions with FLAV content. Nevertheless, the hydrogen bonding structuring of the DES suffers minor disruption upon FLAV solubilization even for high FLAV content because of the versatility of FLAVs to be hydrogen bonded with all the available sites in the DES, thus pairing DES−DES with DES−FLAV interactions. Regarding the FLAV hydrogen bonding with DES components, the number of interactions per FLAV molecule follows the ordering GLY > Cl > Ch, which shows the preference to be interacting with the DES HBD because of the available hydrogen bonding sites. Moreover, FLAV−FLAV hydrogen bonds increase as the FLAV content increases, but even for low FLAV content, FLAV self-association is present.

3.2.5. Domain Analysis. Beyond the nature and extension of hydrogen bonding in the considered mixed fluids, the molecular distribution in the space is also highly relevant because of possible cluster formation. For that purpose, a domain analysis was carried out for the solutions considering the domain count (D; i.e., the number of domains in the fluid with D = 1 indicating a continuous domain), domain volume and area, and isoperimetric index (Q; with Q indicating the sphericity of the domains with values in the 0 to 1 range with Q = 1 indicating perfectly spherical domains) for all the possible molecular domains, Figure 11. The considered domains involve Ch, GLY, and FLAV studied for the type of FLAV and FLAV content effect. The reported results indicate an almost negligible effect of the type of involved FLAV, with all of the considered FLAVs showing the same trends for the different properties. In the case of Ch domains, they show low D values, i.e., a large trend to self-associate into the DES, leading to a continuous distribution of Ch cations into the fluid, with minor disruption because of the FLAV presence. Only for large FLAV content does D for Ch increase: the DES suffers disruption because of the clustering trend of the FLA within content. This effect on Ch distribution is accompanied by a decrease in the volume and area of Ch domains accompanied by an increase of sphericity for Ch clusters. For GLY domains, it shows surprisingly minor changes in the considered FLAV content range; thus, D values are larger than for Ch. That is, GLY has a larger trend to self-associate as it is present in a 1:2 ratio when compared with Ch, and the development of GLY−FLAV hydrogen bonding reported in Figure 10 does not decrease GLY clustering because of the presence of a large number of hydrogen bonding sites. Likewise, GLY domains are not spherical, as indicated by the close to zero Q values. Regarding FLAV domains, D results clearly indicate the trend to decrease its size, evolving from isolated FLAV clusters interacting with DES components to large clusters (lower D) as the FLAV content increases, which confirms SDF results in Figure 7. This FLAV aggregation is then accompanied by an increase in volume and area and a

https://doi.org/10.1021/acsfoodscitech.3c00281
ACS Food Sci. Technol. 2023, 3, 1931−1947

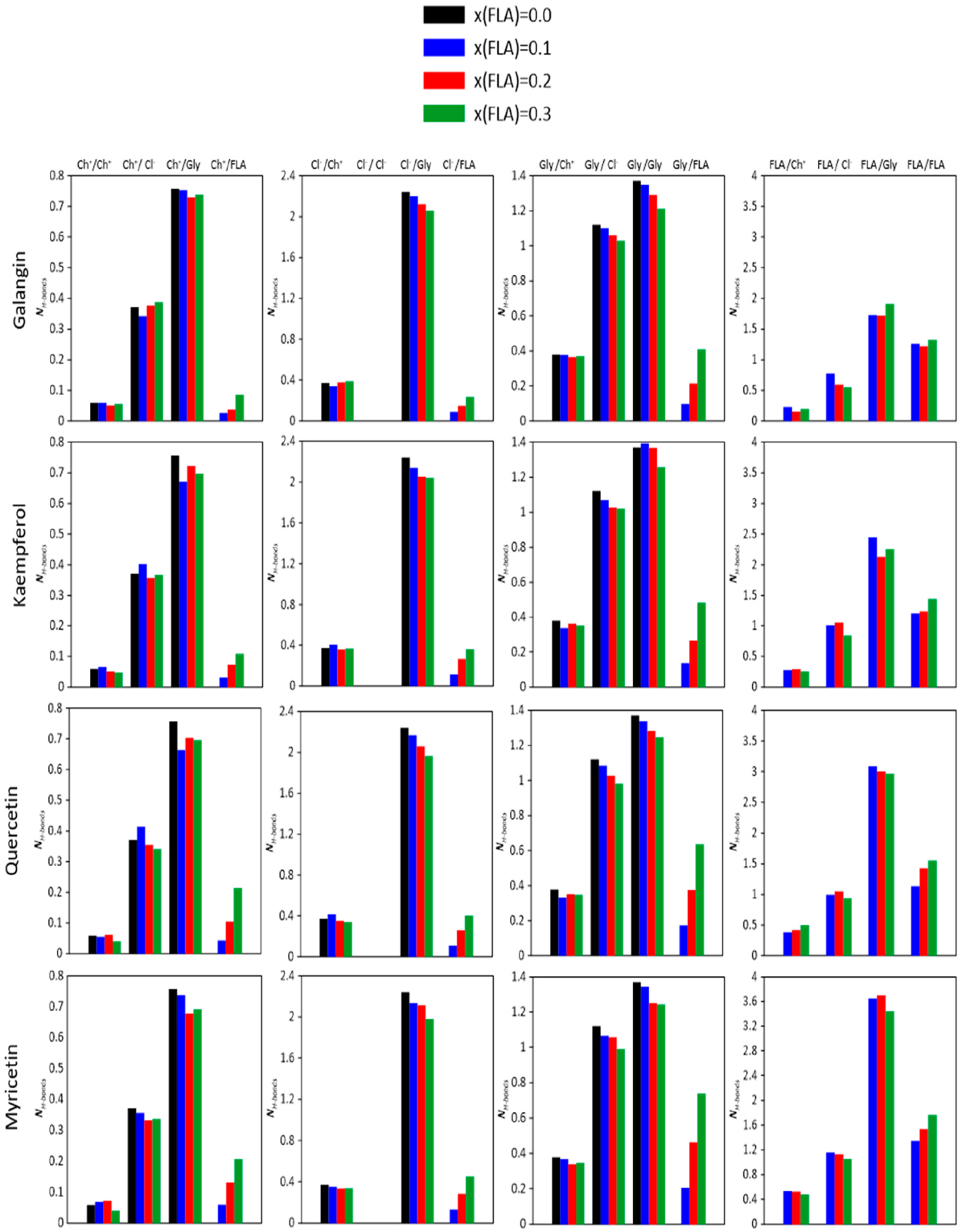

Figure 10. Number of hydrogen bonds, $N_{\text{H-bonds}}$, split for all the available molecular pairs, for x FLAV + $(1 - x)$ DES mixtures as a function of the FLAV content at 303 K and 1 bar. For each interacting pair, all of the possible donor−acceptor sites are considered.

decrease in cluster sphericity as they extend along the whole fluid.

3.2.6. Velocity Distribution and Intermolecular Interaction Energy. The dynamic properties of DES−FLAV systems were analyzed through the calculated velocity distribution functions (VDFs) also calculated for all the available molecules and FLAV concentrations, Figure 12. A clear FLAV content effect is inferred for all of the considered FLAVS: all of the molecules move more slowly as FLAV is solubilized, and this effect increases with the FLAV content. It is also remarkable that for fixed compositions, the VDFs are almost the same for all the involved molecules; i.e., Ch, Cl, GLY, and FLAVs

https://doi.org/10.1021/acsfoodscitech.3c00281
ACS Food Sci. Technol. 2023, 3, 1931−1947

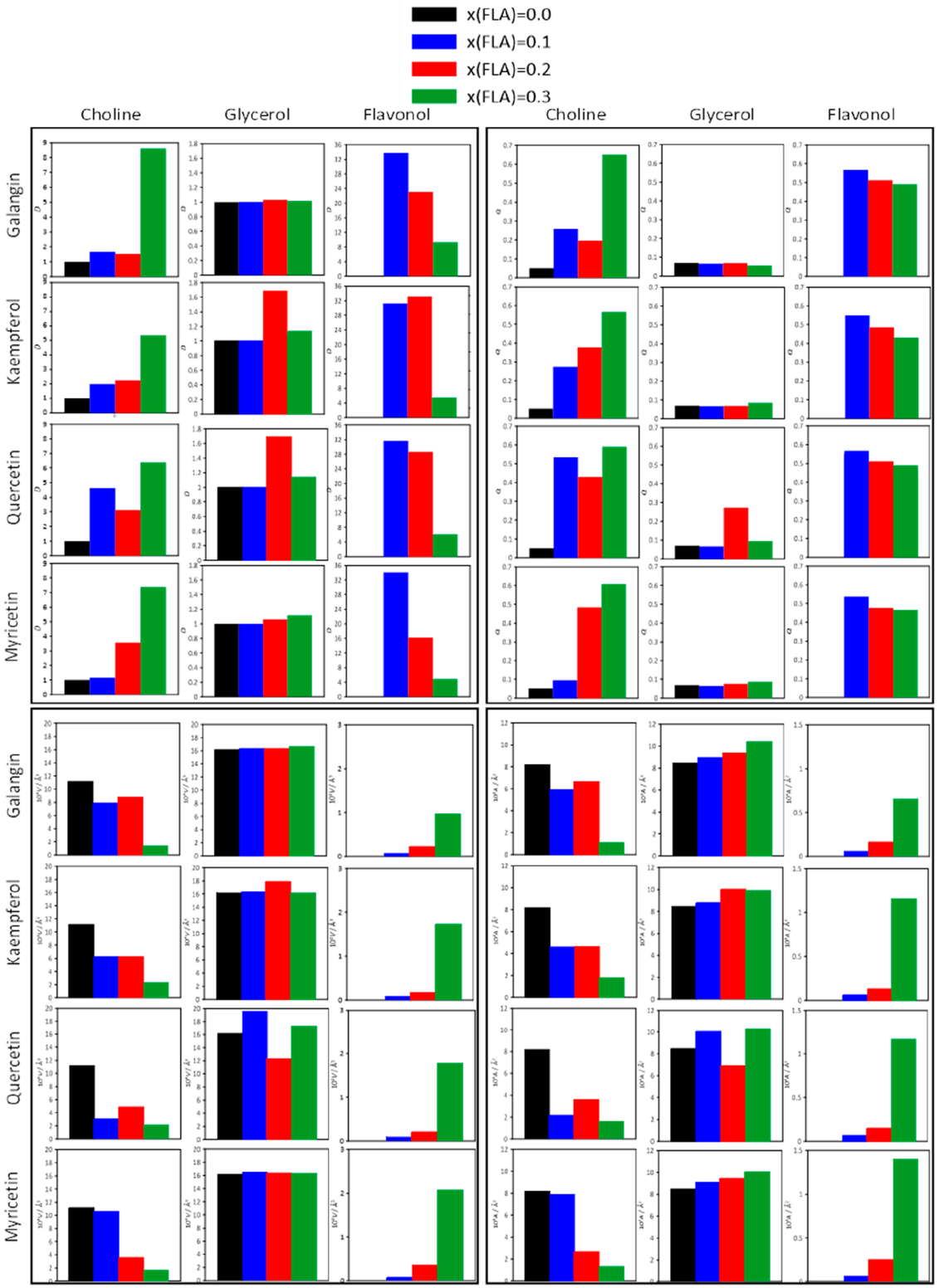

Figure 11. Domain analysis in x FLAV + $(1 - x)$ DES mixtures as a function of the FLAV content at 303 K and 1 bar. Average values for the domain count, D, isoperimetric quotient, Q, domain volume, V, and domain area, A, are reported for each compound.

movements are largely coupled, which is justified considering the extension of hydrogen bonding and the fact that all the molecules are involved in hydrogen bonds with the remaining molecules, Figure 10: a large cooperative hydrogen bonding network is inferred. This hydrogen bonding network is reinforced in the presence of the FLAVs as the presence of these molecules does not largely disrupt the DES self-aggregation, but at the same time, new hydrogen bonds involving FLAVs are formed, thus leading to a decrease in molecular mobility. This effect is confirmed by the intermolecular interaction energies, E_{inter}, reported in Table 3. The reported E_{inter} values indicate a slight decrease for

https://doi.org/10.1021/acsfoodscitech.3c00281
ACS Food Sci. Technol. 2023, 3, 1931−1947

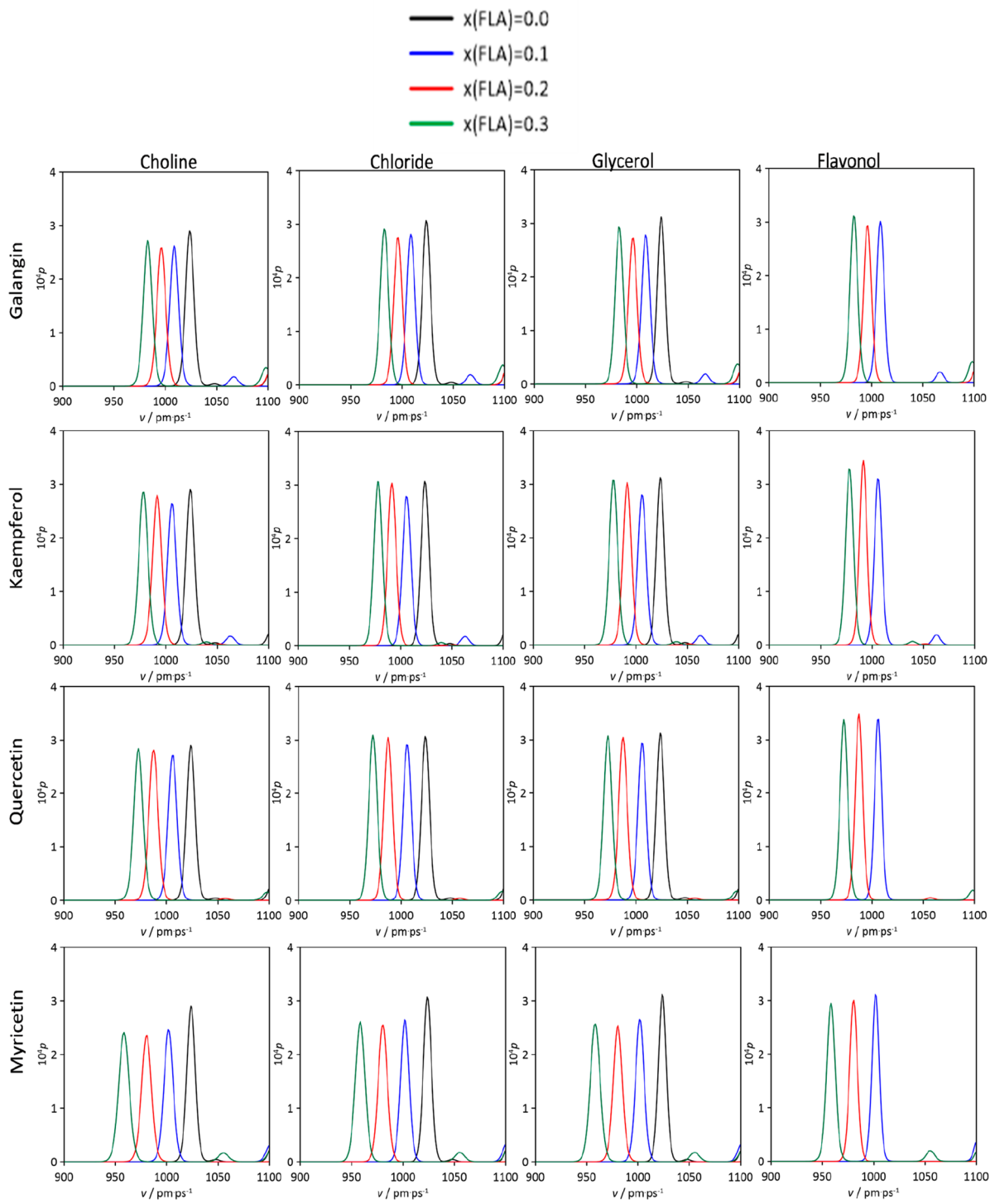

Figure 12. Velocity, v, distribution functions for the reported molecules in x FLAV + $(1 - x)$ DES mixtures as a function of the FLAV content at 303 K and 1 bar.

energies corresponding to interactions between DES components, especially for Ch−Cl ones, but at the same time, GLY−GLY interactions remain almost unchanged, and new interactions involving FLAV molecules, especially GLY−FLA ones, lead to systems with an increase in the total E_{inter}; i.e., the presence of the FLAV reinforces the fluids' structuring because of its ability to develop hydrogen bonds with all the present components.

The reported results clarified the mechanism(s) of flavonols solubilization. The planar structure and, therefore, the π-stacking of the FLAVs in the solid phase prevent their water solubilization. The driving force responsible for the solubilization in ChCl 1:2 Gly is the formation of hydrogen bonds between the solute and the solvent components. The energy of the intermolecular DES-FLAV hydrogen bonds is larger than FLAV−FLAV intermolecular hydrogen bonds, as reported in Table 3, and thus the FLAV−FLAV interactions tend to break

https://doi.org/10.1021/acsfoodscitech.3c00281
ACS Food Sci. Technol. 2023, 3, 1931−1947

Table 3. Intermolecular Interaction Energy, E_{inter}, for the Considered Interacting Pairs in x FLAV + $(1-x)$ DES Mixtures as a Function of FLAV Content at 303 K and 1 bar

		E_{inter}/kJ mol^{-1}						
	x	Ch^+/Cl^-/ kJ·mol^{-1}	Cl^-/Gly/kJ·mol^{-1}	Gly/Gly/kJ·mol^{-1}	Ch^+/FLA/kJ·mol^{-1}	Cl^-/FLA/kJ·mol^{-1}	Gly/FLA/kJ·mol^{-1}	FLA/FLA/kJ·mol^{-1}
ChCl:Gly (1:2)	0	−970.0	−147.0	−40.0	—	—	—	—
				x FLAV + $(1-x)$ ChCl: Gly (1:2)				
x GA + $(1-x)$ ChCl:Gly (1:2)	0.1	−921.7	−151.2	−43.5	−28.8	−32.4	−173.2	−11.6
	0.2	−872.9	−130.4	−50.5	−37.4	−56.2	−113.4	−32.5
	0.3	−806.5	−136.7	−40.6	−46.3	−61.0	−101.0	−19.3
x KM + $(1-x)$ ChCl:Gly (1:2)	0.1	−926.5	−136.6	−48.6	−98.9	−91.4	−129.0	−19.3
	0.2	−842.5	−128.6	−37.0	−39.0	−81.3	−98.8	0.2
	0.3	−788.3	−124.6	−43.1	−54.6	−80.2	−150.8	−17.2
x QE + $(1-x)$ ChCl:Gly (1:2)	0.1	−920.3	−140.9	−42.5	−35.7	−83.4	−236.6	−31.5
	0.2	−857.9	−126.2	−42.5	−77.9	−64.1	−163.3	−31.2
	0.3	−804.7	−122.2	−40.6	−78.4	−65.3	−121.2	−38.1
x MR + $(1-x)$ ChCl:Gly (1:2)	0.1	−914.5	−147.0	−43.7	−45.8	−91.1	−134.6	−0.9
	0.2	−864.5	−138.3	−43.9	−36.6	−70.2	−236.3	−54.0
	0.3	−789.3	−115.7	−44.1	−94.2	−73.7	−174.1	−31.2

in order to pair with DES atoms. It can be understood as the solvent has sufficient energy to break the intermolecular hydrogen bonds established by the solute in the solid phase due to the packing to form new and stronger hydrogen bonds with it. Therefore, MD results indicate that FLAV solubilization is produced by the large ability of FLAV molecules to develop hydrogen bonds with any of the DES components, especially with GLY, with minor disruption of the DES structuring, and only when FLAVs concentration is large enough to saturate all the available DES hydrogen bonding sites do the FLAVs tend to form large self-aggregates which would be on the root of phase separation and the FLAV solubility limit in the considered DES.

Therefore, deep eutectic solvents with suitable hydrogen bonding ability may be considered as platforms for flavonol extraction from natural sources alternative to their low solubility in common solvents. The design of solvents with a suitable hydrogen bonding ability with the available sites in the flavonols could be used to improve their performance and reach higher extraction.

For the proper design of suitable DESs and to achieve better solubilization of flavonols in deep eutectic solvents (DES), several key factors and recommendations have been identified from the research:

(1) Hydrogen bonding capability: The primary factor governing flavonol solubilization in DES is the ability to form effective hydrogen bonds. DES components, including hydrogen bond acceptors (HBA) and hydrogen bond donors (HBD), play a crucial role in facilitating these interactions.

(2) Hydroxyl group position: Flavonols contain hydroxyl groups located at various positions on their aromatic rings. Hydroxyl groups, especially those in the cathecol moiety, are key sites for hydrogen bonding and should be strategically considered when designing DES for flavonol solubilization.

(3) Ketone and ether groups: While hydroxyl groups can act as both hydrogen bond donors and acceptors, the oxygen atoms in ketone and ether groups primarily serve as hydrogen bond acceptors. Understanding the role of these groups is essential in designing effective DES for flavonol solubilization.

(4) Structural modifications: Exploring structural modifications to flavonols can enhance their solubility in DES. These modifications should aim to optimize the interaction between flavonols and DES components.

(5) DES composition: Carefully selecting the components and ratios of the DES is critical. Researchers should assess various DES compositions to identify those with the highest solubilizing capacity for specific flavonols.

(6) Temperature control: Controlling temperature conditions is vital to ensure that the DES operates within its ideal solubility range. Adjusting the temperature can help enhance flavonol solubility.

In summary, achieving better solubilization of flavonols in DES involves optimizing hydrogen bonding interactions, considering the position of hydroxyl groups and carefully designing the DES composition.

■ ASSOCIATED CONTENT

Supporting Information

The Supporting Information is available free of charge at https://pubs.acs.org/doi/10.1021/acsfoodscitech.3c00281.

Table S1 (force field parametrizations for MD simulations used along this work; parameters for all the considered molecules are reported in this table) (PDF)

■ AUTHOR INFORMATION

Corresponding Authors

Mert Atilhan − *Department of Chemical and Paper Engineering, Western Michigan University, Kalamazoo, Michigan 49008-5462, United States;* orcid.org/0000-0001-8270-7904; Email: mert.atilhan@wmich.edu

Santiago Aparicio − *Department of Chemistry and International Research Centre in Critical Raw Materials-*

https://doi.org/10.1021/acsfoodscitech.3c00281
ACS Food Sci. Technol. 2023, 3, 1931−1947

ICCRAM, University of Burgos, 09001 Burgos, Spain; orcid.org/0000-0001-9996-2426; Email: sapar@ubu.es

Authors

Nuria Aguilar − *Department of Chemistry, University of Burgos, 09001 Burgos, Spain;* orcid.org/0000-0002-9339-4330

Alfredo Bol-Arreba − *International Research Centre in Critical Raw Materials-ICCRAM and Department of Physics, University of Burgos, 09001 Burgos, Spain;* orcid.org/0000-0003-4641-4826

Complete contact information is available at: https://pubs.acs.org/10.1021/acsfoodscitech.3c00281

Notes

The authors declare no competing financial interest.

■ ACKNOWLEDGMENTS

We acknowledge SCAYLE (Supercomputación Castilla y León, Spain) for providing supercomputing facilities. The statements made herein are solely the responsibility of the authors. The authors declare no competing interests.

■ REFERENCES

(1) Hansen, B. B.; Spittle, S.; Chen, B.; Poe, D.; Zhang, Y.; Klein, J. M.; Horton, A.; Adhikari, L.; Zelovich, T.; Doherty, B. W.; Gurkan, B.; Maginn, E. J.; Ragauskas, A.; Dadmun, M.; Zawodzinski, T. A.; Baker, G. A.; Tuckerman, M. E.; Savinell, R. F.; Sangoro, J. R. Deep Eutectic Solvents: A Review Of Fundamentals And Applications. *Chem. Rev.* **2021**, *121*, 1232−1285.

(2) Vanda, H.; Dai, Y.; Wilson, E. G.; Verpoorte, R.; Choi, Y. H. Green Solvents From Ionic Liquids And Deep Eutectic Solvents To Natural Deep Eutectic Solvents. *Comptes Rendus Chimie* **2018**, *21*, 628−638.

(3) Smith, E. L.; Abbott, A. P.; Ryder, K. S. Deep Eutectic Solvents (Dess) And Their Applications. *Chem. Rev.* **2014**, *114*, 11060−11082.

(4) Gurkan, B. E.; Maginn, E. J.; Pentzer, E. B. Deep Eutectic Solvents: A New Class Of Versatile Liquids. *J. Phys. Chem. B* **2020**, *124*, 11313−11315.

(5) Abbott, A. P.; Capper, G.; Davies, D. L.; Rasheed, R. K.; Tambyrajah, V. Novel Solvent Properties Of Choline Chloride/Urea Mixtures. *Chem. Commun.* **2003**, *1*, 70−71.

(6) You, Y. H.; Gu, C. D.; Wang, X. L.; Tu, J. P. Electrodeposition Of Ni−Co Alloys From A Deep Eutectic Solvent. *Surf. Coat. Technol.* **2012**, *206*, 3632−3638.

(7) Jenkin, G. R. T.; Al-Bassam, A. Z. M.; Harris, R. C.; Abbott, A. P.; Smith, D. J.; Holwell, D. A.; Chapman, R. J.; Stanley, C. J. The Application Of Deep Eutectic Solvent Ionic Liquids For Environmentally-Friendly Dissolution And Recovery Of Precious Metals. *Minerals Engineering* **2016**, *87*, 18−24.

(8) Warrag, S. E. E.; Peters, C. J.; Kroon, M. C. Deep Eutectic Solvents For Highly Efficient Separations In Oil And Gas Industries. *Current Opinion In Green And Sustainable Chemistry* **2017**, *5*, 55−60.

(9) García, G.; Aparicio, S.; Ullah, R.; Atilhan, M. Deep Eutectic Solvents: Physicochemical Properties And Gas Separation Applications. *Energy Fuels* **2015**, *29*, 2616−2644.

(10) Ma, C.; Sarmad, S.; Mikkola, J.-P.; Ji, X. Development Of Low-Cost Deep Eutectic Solvents For Co2 Capture. *Energy Procedia* **2017**, *142*, 3320−3325.

(11) Ren, H.; Lian, S.; Wang, X.; Zhang, Y.; Duan, E. Exploiting The Hydrophilic Role Of Natural Deep Eutectic Solvents For Greening Co_2 Capture. *Journal Of Cleaner Production* **2018**, *193*, 802−810.

(12) Li, C.; Li, D.; Zou, S.; Li, Z.; Yin, J.; Wang, A.; Cui, Y.; Yao, Z.; Zhao, Q. Extraction Desulfurization Process Of Fuels With Ammonium-Based Deep Eutectic Solvents. *Green Chem.* **2013**, *15*, 2793−2799.

(13) Atilhan, M.; Aparicio, S. Review And Perspectives For Effective Solutions To Grand Challenges Of Energy And Fuels Technologies Via Novel Deep Eutectic Solvents. *Energy Fuels* **2021**, *35*, 6402−6419.

(14) Zhao, H.; Zhang, C.; Crittle, T. D. Choline-Based Deep Eutectic Solvents For Enzymatic Preparation Of Biodiesel From Soybean Oil. *Journal Of Molecular Catalysis B: Enzymatic* **2013**, *85*−*86*, 243−247.

(15) Sander, A.; Petračić, A.; Parlov Vuković, J.; Husinec, L. From Coffee To Biodiesel—Deep Eutectic Solvents For Feedstock And Biodiesel Purification. *Separations* **2020**, *7*, 22.

(16) Maugeri, Z.; Domínguez De María, P. Whole-Cell Biocatalysis In Deep-Eutectic-Solvents/Aqueous Mixtures. *Chem. Catal. Chem.* **2014**, *6*, 1535−1537.

(17) Liu, P.; Hao, J. W.; Mo, L. P.; Zhang, Z. H. Recent Advances In The Application Of Deep Eutectic Solvents As Sustainable Media As Well As Catalysts In Organic Reactions. *Rsc Adv.* **2015**, *5*, 48675−48704.

(18) Hayyan, M.; Mjalli, F. S.; Hashim, M. A.; Alnashef, I. M. A Novel Technique For Separating Glycerine From Palm Oil-Based Biodiesel Using Ionic Liquids. *Fuel Process. Technol.* **2010**, *91*, 116−120.

(19) Xia, S.; Baker, G. A.; Li, H.; Ravula, S.; Zhao, H. Aqueous Ionic Liquids And Deep Eutectic Solvents For Cellulosic Biomass Pretreatment And Saccharification. *Rsc Adv.* **2014**, *4*, 10586.

(20) Roda, A.; Santos, F.; Matias, A. A.; Paiva, A.; Duarte, A. R. C. Design And Processing Of Drug Delivery Formulations Of Therapeutic Deep Eutectic Systems For Tuberculosis. *Journal Of Supercritical Fluids* **2020**, *161*, No. 104826.

(21) Wikene, K. O.; Rukke, H. V.; Bruzell, E.; Tønnesen, H. H. Investigation Of The Antimicrobial Effect Of Natural Deep Eutectic Solvents (Nades) As Solvents In Antimicrobial Photodynamic Therapy. *Journal Of Photochemistry And Photobiology B: Biology* **2017**, *171*, 27−33.

(22) Silva, E.; Oliveira, F.; Silva, J. M.; Matias, A.; Reis, R. L.; Duarte, A. R. C. Optimal Design Of Thedes Based On Perillyl Alcohol And Ibuprofen. *Pharmaceutics* **2020**, *12*, 1121.

(23) Shekaari, H.; Zafarani-Moattar, M. T.; Shayanfar, A.; Mokhtarpour, M. Effect Of Choline Chloride/Ethylene Glycol Or Glycerol As Deep Eutectic Solvents On The Solubility And Thermodynamic Properties Of Acetaminophen. *Journal Of Molecular Liquids* **2018**, *249*, 1222−1235.

(24) Gutiérrez, A.; Atilhan, M.; Aparicio, S. Behavior Of Antibiotics In Natural Deep Eutectic Solvents. *J. Chem. Eng. Data* **2020**, *65*, 4669−4683.

(25) Gutiérrez, A.; Atilhan, M.; Aparicio, S. Theoretical Study On Deep Eutectic Solvents As Vehicles For The Delivery Of Anesthetics. *J. Phys. Chem. B* **2020**, 11756.

(26) Aroso, I. M.; Craveiro, R.; Rocha, Â.; Dionísio, M.; Barreiros, S.; Reis, R. L.; Paiva, A.; Duarte, A. R. C. Design Of Controlled Release Systems For Thedes—Therapeutic Deep Eutectic Solvents, Using Supercritical Fluid Technology. *International Journal Of Pharmaceutics* **2015**, *492*, 73−79.

(27) Paradiso, V. M.; Clemente, A.; Summo, C.; Pasqualone, A.; Caponio, F. Towards Green Analysis Of Virgin Olive Oil Phenolic Compounds: Extraction By A Natural Deep Eutectic Solvent And Direct Spectrophotometric Detection. *Food Chem.* **2016**, *212*, 43−47.

(28) Jeong, K. M.; Ko, J.; Zhao, J.; Jin, Y.; Yoo, D. E.; Han, S. Y.; Lee, J. Multi-Functioning Deep Eutectic Solvents As Extraction And Storage Media For Bioactive Natural Products That Are Readily Applicable To Cosmetic Products. *Journal Of Cleaner Production* **2017**, *151*, 87−95.

(29) Soltanmohammadi, F.; Jouyban, A.; Shayanfar, A. New Aspects Of Deep Eutectic Solvents: Extraction, Pharmaceutical Applications, As Catalyst And Gas Capture. *Chemical Papers* **2021**, *75*, 439−453.

(30) Radošević, K.; Bubalo, M. C.; Srček A, V. G.; Grgas, D.; Dragičević, T. L.; Redovniković, I. R. Evaluation Of Toxicity And Biodegradability Of Choline Chloride Based Deep Eutectic Solvents. *Ecotoxicology Environmental Safety* **2015**, *112*, 46−53.

(31) Abbott, A. P.; Harris, R. C.; Ryder, K. S.; D'agostino, C.; Gladden, L. F.; Mantle, M. D. Glycerol Eutectics As Sustainable Solvent Systems. *Green Chem.* **2011**, *13*, 82−90.
(32) Huang, J.; Guo, X.; Xu, T.; Fan, L.; Zhou, X.; Wu, S. Ionic Deep Eutectic Solvents For The Extraction And Separation Of Natural Products. *Journal Of Chromatography A* **2019**, *1598*, 1−19.
(33) Yadav, A.; Trivedi, S.; Rai, R.; Pandey, S. Densities And Dynamic Viscosities Of (Choline Chloride + Glycerol) Deep Eutectic Solvent And Its Aqueous Mixtures In The Temperature Range (283.15−363.15) K. *Fluid Phase Equilib.* **2014**, *367*, 135−142.
(34) Shahbaz, K.; Baroutian, S.; Mjalli, F. S.; Hashim, M. A.; Alnashef, I. M. Densities Of Ammonium And Phosphonium Based Deep Eutectic Solvents: Prediction Using Artificial Intelligence And Group Contribution Techniques. *Thermochim. Acta* **2012**, *527*, 59−66.
(35) AlOmar, M. K.; Hayyan, M.; Alsaadi, M. A.; Akib, S.; Hayyan, A.; Hashim, M. A. Glycerol-Based Deep Eutectic Solvents: Physical Properties. *J. Mol. Liq.* **2016**, *215*, 98−103.
(36) Li, X.; Row, K. H. Development Of Deep Eutectic Solvents Applied In Extraction And Separation. *J. Sep. Science* **2016**, *39*, 3505−3520.
(37) Chen, J.; Li, Y.; Wang, X.; Liu, W. Application Of Deep Eutectic Solvents In Food Analysis: A Review. *Molecules* **2019**, *24*, 4594.
(38) Ruesgas-Ramón, M.; Figueroa-Espinoza, M. C.; Durand, E. Application Of Deep Eutectic Solvents (Des) For Phenolic Compounds Extraction: Overview, Challenges, And Opportunities. *J. Agric. Food Chem.* **2017**, *65*, 3591−3601.
(39) Cunha, S. C.; Fernandes, J. O. Extraction Techniques With Deep Eutectic Solvents. *Trac Trends In Analytical Chemistry* **2018**, *105*, 225−239.
(40) Serna-Vázquez, J.; Ahmad, M. Z.; Boczkaj, G.; Castro-Muñoz, R. Latest Insights On Novel Deep Eutectic Solvents (Des) For Sustainable Extraction Of Phenolic Compounds From Natural Sources. *Molecules* **2021**, *26*, 5037.
(41) Górniak, I.; Bartoszewski, R.; Króliczewski, J. Comprehensive Review Of Antimicrobial Activities Of Plant Flavonoids. *Phytochem Rev.* **2019**, *18*, 241−272.
(42) Brodowska, K. M. Natural Flavonoids: Classification, Potential Role, And Application Of Flavonoid. *Analogues* **2017**, *7* (2), 108−123.
(43) Nagula, R. L.; Wairkar, S. Recent Advances In Topical Delivery Of Flavonoids: A Review. *Journal Of Controlled Release* **2019**, *296*, 190−201.
(44) Rodríguez-García, C.; Sánchez-Quesada, C.; Gaforio, J. J. Dietary Flavonoids As Cancer Chemopreventive Agents: An Updated Review Of Human Studies. *Antioxidants* **2019**, *8*, 137.
(45) Skarpalezos, D.; Detsi, A. Deep Eutectic Solvents As Extraction Media For Valuable Flavonoids From Natural Sources. *Appl. Sci.* **2019**, *9* (19), 4169.
(46) Cai, X.; Xiao, M.; Zou, X.; Tang, J.; Huang, B.; Xue, H. Extraction And Separation Of Flavonoids From *Malus Hupehensis* Using High-Speed Countercurrent Chromatography Based On Deep Eutectic Solvent. *Journal Of Chromatography A* **2021**, *1641*, No. 461998.
(47) Mansur, A. R.; Song, N.-E.; Jang, H. W.; Lim, T.-G.; Yoo, M.; Nam, T. G. Optimizing The Ultrasound-Assisted Deep Eutectic Solvent Extraction Of Flavonoids In Common Buckwheat Sprouts. *Food Chem.* **2019**, *293*, 438−445.
(48) Ali, M. C.; Chen, J.; Zhang, H.; Li, Z.; Zhao, L.; Qiu, H. Effective Extraction Of Flavonoids From *Lycium Barbarum L.* Fruits By Deep Eutectic Solvents-Based Ultrasound-Assisted Extraction. *Talanta* **2019**, *203*, 16−22.
(49) Xu, M.; Ran, L.; Chen, N.; Fan, X.; Ren, D.; Yi, L. Polarity-Dependent Extraction Of Flavonoids From Citrus Peel Waste Using A Tailor-Made Deep Eutectic Solvent. *Food Chem.* **2019**, *297*, No. 124970.
(50) Shang, X.; Dou, Y.; Zhang, Y.; Tan, J.-N.; Liu, X.; Zhang, Z. Tailor-Made Natural Deep Eutectic Solvents For Green Extraction Of Isoflavones From Chickpea (*Cicer Arietinum L.*) Sprouts. *Industrial Crops And Products* **2019**, *140*, No. 111724.
(51) Xia, G.-H.; Li, X.-H.; Jiang, Y. Deep Eutectic Solvents As Green Media For Flavonoids Extraction From The Rhizomes Of *Polygonatum Odoratum*. *Alexandria Engineering Journal* **2021**, *60*, 1991−2000.
(52) Ozturk, B.; Parkinson, C.; Gonzalez-Miquel, M. Extraction Of Polyphenolic Antioxidants From Orange Peel Waste Using Deep Eutectic Solvents. *Separation And Purification Technology* **2018**, *206*, 1−13.
(53) Cao, D.; Liu, Q.; Jing, W.; Tian, H.; Yan, H.; Bi, W.; Jiang, Y.; Chen, D. D. Y. Insight Into The Deep Eutectic Solvent Extraction Mechanism Of Flavonoids From Natural Plant. *Acs Sustainable Chem. Eng.* **2020**, *8*, 19169−19177.
(54) Wang, H.; Liu, S.; Zhao, Y.; Wang, J.; Yu, Z. Insights Into The Hydrogen Bond Interactions In Deep Eutectic Solvents Composed Of Choline Chloride And Polyols. *Acs Sustainable Chem. Eng.* **2019**, *7*, 7760−7767.
(55) Gutiérrez, A.; Alcalde, R.; Atilhan, M.; Aparicio, S. Insights On Betaine + Lactic Acid Deep Eutectic Solvent. *Ind. Eng. Chem. Res.* **2020**, *59*, 11880−11892.
(56) Bi, W.; Tian, M.; Row, K. H. Evaluation Of Alcohol-Based Deep Eutectic Solvent In Extraction And Determination Of Flavonoids With Response Surface Methodology Optimization. *Journal Of Chromatography A* **2013**, *1285*, 22−30.
(57) Qi, X.-L.; Peng, X.; Huang, Y.-Y.; Li, L.; Wei, Z.-F.; Zu, Y.-G.; Fu, Y.-J. Green And Efficient Extraction Of Bioactive Flavonoids From *Equisetum Palustre L.* By Deep Eutectic Solvents-Based Negative Pressure Cavitation Method Combined With Macroporous Resin Enrichment. *Industrial Crops And Products* **2015**, *70*, 142−148.
(58) Wang, G.; Cui, Q.; Yin, L.-J.; Zheng, X.; Gao, M.-Z.; Meng, Y.; Wang, W. Efficient Extraction Of Flavonoids From *Flos Sophorae Immaturus* By Tailored And Sustainable Deep Eutectic Solvent As Green Extraction Media. *Journal Of Pharmaceutical And Biomedical Analysis* **2019**, *170*, 285−294.
(59) Meng, Z.; Zhao, J.; Duan, H.; Guan, Y.; Zhao, L. Green And Efficient Extraction Of Four Bioactive Flavonoids From *Pollen Typhae* By Ultrasound-Assisted Deep Eutectic Solvents Extraction. *Journal Of Pharmaceutical And Biomedical Analysis* **2018**, *161*, 246−253.
(60) Li, X.; Row, K. H. Preparation Of Deep Eutectic Solvent-Based Hexagonal Boron Nitride-Molecularly Imprinted Polymer Nanoparticles For Solid Phase Extraction Of Flavonoids. *Microchim Acta* **2019**, *186*, 753.
(61) Adams, S.; De Castro, P.; Echenique, P.; Estrada, J.; Hanwell, M. D.; Murray-Rust, P.; Sherwood, P.; Thomas, J.; Townsend, J. The Quixote Project: Collaborative And Open Quantum Chemistry Data Management In The Internet Age. *J. Cheminform.* **2011**, *3*, 38.
(62) Neese, F. The Orca Program System. *Wires Comput. Mol. Sci.* **2012**, *2*, 73−78.
(63) Chai, J.-D.; Head-Gordon, M. Systematic Optimization Of Long-Range Corrected Hybrid Density Functionals. *J. Chemical Physics* **2008**, *128*, No. 084106.
(64) Schäfer, A.; Huber, C.; Ahlrichs, R. Fully Optimized Contracted Gaussian Basis Sets Of Triple Zeta Valence Quality For Atoms Li To Kr. *Journal Of Chemical Physics* **1994**, *100*, 5829−5835.
(65) Weigend, F. Accurate Coulomb-Fitting Basis Sets For H To Rn. *Phys. Chem. Chem. Phys.* **2006**, *8*, 1057.
(66) Bader, R. F. W. *Atoms In Molecules: A Quantum Theory*; Oxford University Press, 1990.
(67) Lu, T.; Chen, F. Multiwfn: A Multifunctional Wavefunction Analyzer. *J. Comput. Chem.* **2012**, *33*, 580−592.
(68) Fuster, F.; Silvi, B. Does The Topological Approach Characterize The Hydrogen Bond? *Theor. Chem. Acc.* **2000**, *104*, 13−21.
(69) Contreras-García, J.; Johnson, E. R.; Keinan, S.; Chaudret, R.; Piquemal, J.-P.; Beratan, D. N.; Yang, W. Nciplot: A Program For Plotting Noncovalent Interaction Regions. *J. Chem. Theory Comput.* **2011**, *7*, 625−632.

https://doi.org/10.1021/acsfoodscitech.3c00281
ACS Food Sci. Technol. 2023, 3, 1931−1947

(70) Lyubartsev, A. P.; Laaksonen, A. M.Dynamix − A Scalable Portable Parallel Md Simulation Package For Arbitrary Molecular Mixtures. *Comput. Phys. Commun.* **2000**, *128*, 565−589.
(71) Zoete, V.; Cuendet, M. A.; Grosdidier, A.; Michielin, O. Swissparam: A Fast Force Field Generation Tool For Small Organic Molecules. *J. Comput. Chem.* **2011**, *32*, 2359−2368.
(72) Breneman, C. M.; Wiberg, K. B. Determining atom-centered monopoles from molecular electrostatic potentials. The need for high sampling density in formamide conformational analysis. *J. Comput. Chem.* **1990**, *11*, 361−373.
(73) Evans, D. J.; Holian, B. L. The Nose−Hoover Thermostat. *J. Chem. Phys.* **1985**, *83*, 4069.
(74) Essmann, U.; Perera, L.; Berkowitz, M. L.; Darden, T.; Lee, H.; Pedersen, L. G. A Smooth Particle Mesh Ewald Method. *Journal Of Chemical Physics* **1995**, *103*, 8577−8593.
(75) Tuckerman, M.; Berne, B. J.; Martyna, G. J. Reversible Multiple Time Scale Molecular Dynamics. *Journal Of Chemical Physics* **1992**, *97*, 1990−2001.
(76) Humphrey, W.; Dalke, A.; Schulten, K. Vmd - Visual Molecular Dynamics. *J. Mol. Graphics* **1996**, *14*, 33−38.
(77) Brehm, M.; Kirchner, B. Travis - A Free Analyzer And Visualizer For Monte Carlo And Molecular Dynamics Trajectories. *J. Chem. Inf. Model.* **2011**, *51*, 2007−2023.
(78) Koch, U.; Popelier, L. A. Characterization Of C-H-O Hydrogen Bonds On The Basis Of Charge Density. *J. Phys. Chem.* **1995**, *99*, 9747−9754.

https://doi.org/10.1021/acsfoodscitech.3c00281
ACS Food Sci. Technol. 2023, 3, 1931−1947